Hindawi
International Journal of RF and Microwave Computer-Aided Engineering
Volume 2023, Article ID 8827119, 7 pages
https://doi.org/10.1155/2023/8827119

Research Article

A Sub-6 GHz Switching System for Simultaneous Use of 2-Port Network Analyzer by 4 Users

Youna Jang,[1] **Chang In Baek**,[2] **Dong Min Kim**,[1] **Dal Ahn**,[1] **and Seong-Ho Son**[1]

[1]*Department of ICT Convergence, Soonchunhyang University, Asan 31538, Republic of Korea*
[2]*Erangtek, Hwaseong 31538, Republic of Korea*

Correspondence should be addressed to Seong-Ho Son; son@sch.ac.kr

Received 24 April 2023; Revised 13 November 2023; Accepted 7 December 2023; Published 22 December 2023

Academic Editor: Mangal Sain

A vector network analyzer (VNA) is an expensive and essential device for measuring the scattering coefficients of RF devices in the research and development of microwave systems. However, these VNAs are limited in that they can be only used by one user. To address this limitation, this paper presents a switching system that allows multiple users to measure each device under test using a single VNA at the same time. In particular, a four-user switching system is developed in this study. It is important to calibrate the differences between each channel that inevitably arise during implementation. For calibration, we propose and implement a technique for de-embedding the uneven characteristics between these channels. Its performance is validated by measuring insertion loss, reflection loss, and isolation for the developed switching system.

1. Introduction

The switch matrix is an array that connects signals coming in from a vector network analyzer (VNA) to different ports through an internal switch so that a single port can replace the roles of multiple ports. The commonly used switch matrix systems increase the number of device-under-test (DUT) ports, thus allowing one user to measure the scattering coefficient of multiple DUTs.

However, there is a limitation to this type of system in that only a single user can use a VNA, as different users cannot measure the scattering coefficient data of each DUT.

The use of a VNA in multiport systems requires measurements between all paths of conventional scattering coefficients [1–7]. Moreover, the stability of devices, such as cables and connectors, which are external components, affects the quality of the resulting measurements [8].

Due to its structural characteristics, the method of increasing the receiving port requires technical skills to consider the measurement methods and error and test equipment limitations.

As the number of ports increases, the cost of the device must also be taken into account. This means that VNAs are not insignificant to popular manufacturers, such as Keysight Technologies, Rohde & Schwarz, and Anritsu [9]. Two different de-embedding algorithms for RF measurements [10] have been presented, but they are only for one user.

Therefore, this study is aimed at designing and implementing a new switching system that allows multiple users to work on a switch matrix so that four users can simultaneously measure the scattering coefficient data of a DUT.

2. Design of Switch Matrix for Multiple Users

2.1. Design and Fabrication. Figure 1 shows the proposed switching system for simultaneous use of a single VNA by 4 users. Here, the multiuser switch matrix is presented in Figure 2. As shown in Figure 2(a), on the left side of the switch arrangement, three single-pole double-throw (SPDT) switches are arranged with a two-stage connection to distribute one port of the VNA into four ports. On the right, three SPDT switches are arranged in the same way to provide four ports. The dual-switch structure measures *S*-parameter data from four DUTs with a single two-port VNA.

The multiuser switch matrix is interconnected using absorptive SPDTs working at 0.5–6 GHz (Mini-Circuits,

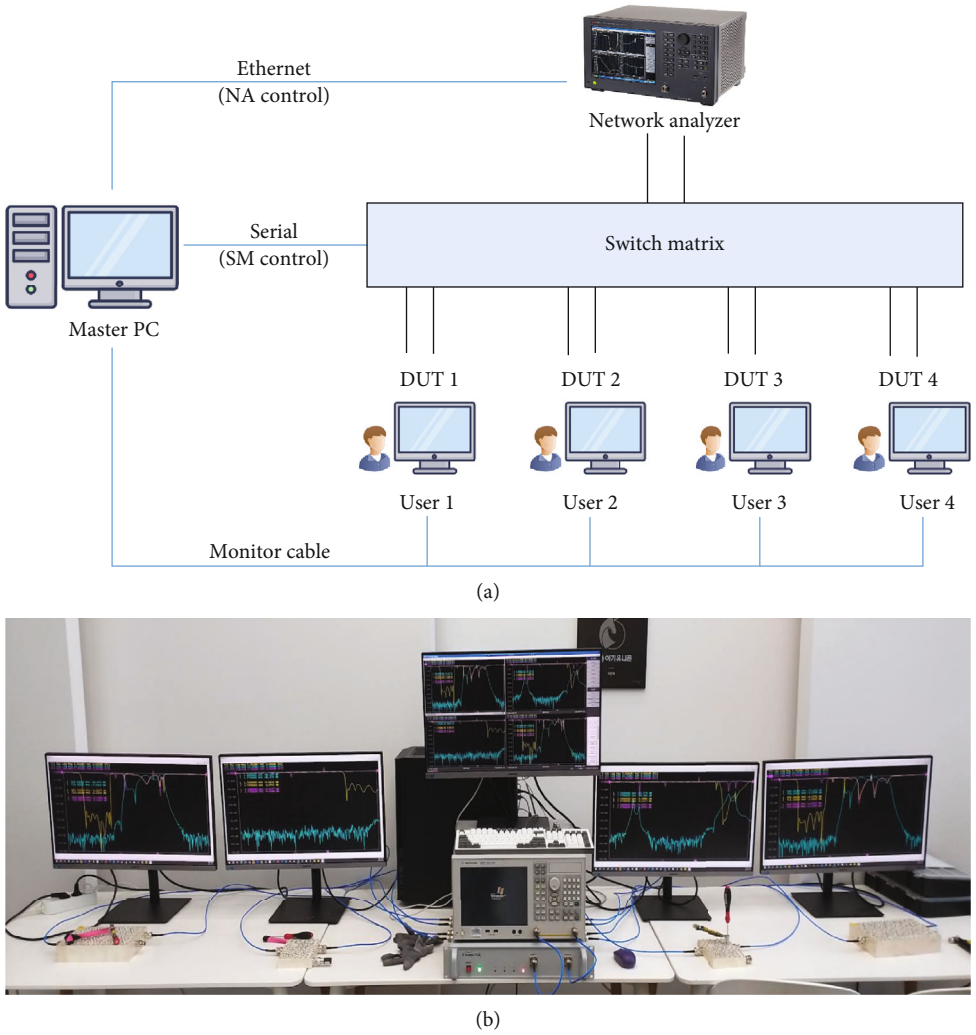

FIGURE 1: (a) Conceptual diagram and (b) realization of a switching system for simultaneous use of a single VNA.

ZFSWA2R-63DR+ [11]) and a microcontroller (Arduino Uno). The SPDT switch elements are connected to each other to create a path to branch 1 channel (2 ports of the VNA) into 4 channels (2 ports/channel). The microcontroller then alternately turns on one of the four channels (and off the remaining channels) at high speed. A light-emitting diode module was used to check the operation. In addition, sufficient power for each component is provided by Arduino's power output, but a power supply was used for spare power. The RF connectors used a Sub-Miniature version A (SMA) type. Finally, the multiuser switch matrix was implemented, as shown in Figure 2(b). The proposed system is set up with five monitors (one master and four user monitors) connected to a single desktop. Each user can view each monitor (4 monitors in total) connected to the desktop and perform their own tuning work. The proposed system allows four users to access a single VNA simultaneously and measure their DUTs, as shown in Figure 1.

2.2. Channel Performance. The channel performance of the manufactured multiuser switch matrix must be checked. If the insertion loss and the reflection loss differ between ports, then even if four people tune the same filter, each product will have a different performance, which ultimately affects product quality. It is also important to check the degree of isolation because when the frequency increases, coupling occurs in which the microwave signal passes from the cable to another cable. When interference occurs, the scattering coefficients affect each other, distorting the scattering coefficients displayed to the user and affecting product quality, such as when the insertion loss and the return loss do not match at each port.

2.2.1. Insertion Loss. The insertion loss represents a value that is lost internally as the signal passes through an element or circuit. Figure 3(a) shows the insertion loss of the Tx stage path composed of A-A_n, and Figure 3(b) shows the insertion loss of the Rx stage path composed of B-B_n, where n is 1, 2, 3, and 4. The four Tx and Rx stage paths show different insertion loss performances at 0–6.0 GHz, indicating a distortion of insertion loss at a certain point when passing through several RF switches, RF cables, and RF connectors. The insertion loss rapidly increases when it is higher than

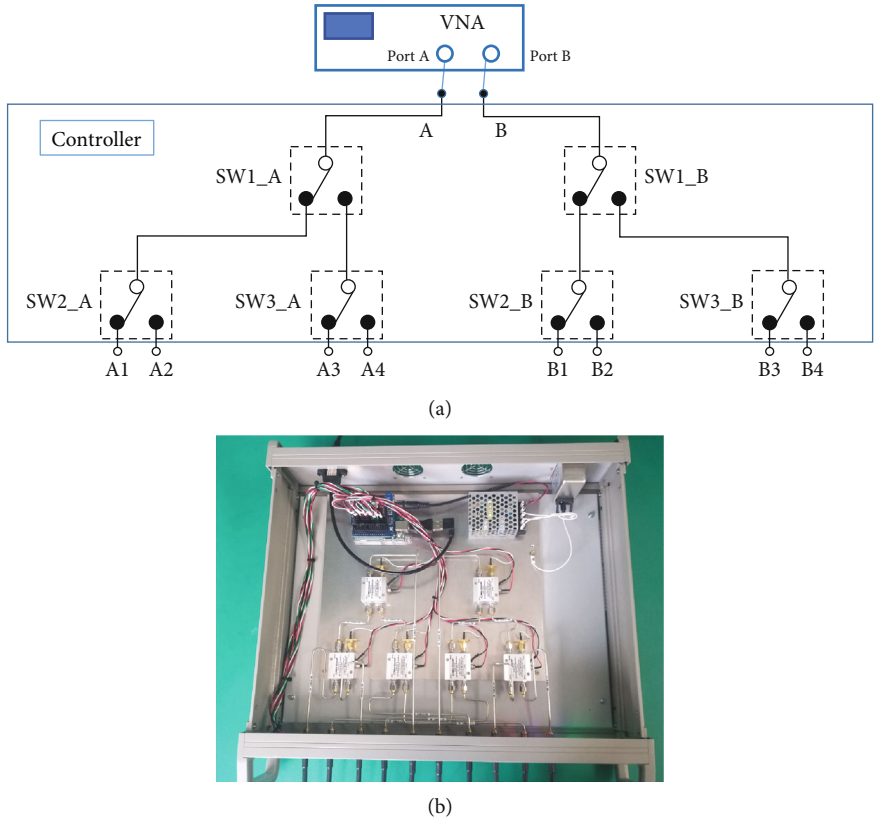

Figure 2: (a) Internal schematic and (b) implemented configuration of a switching matrix for four users.

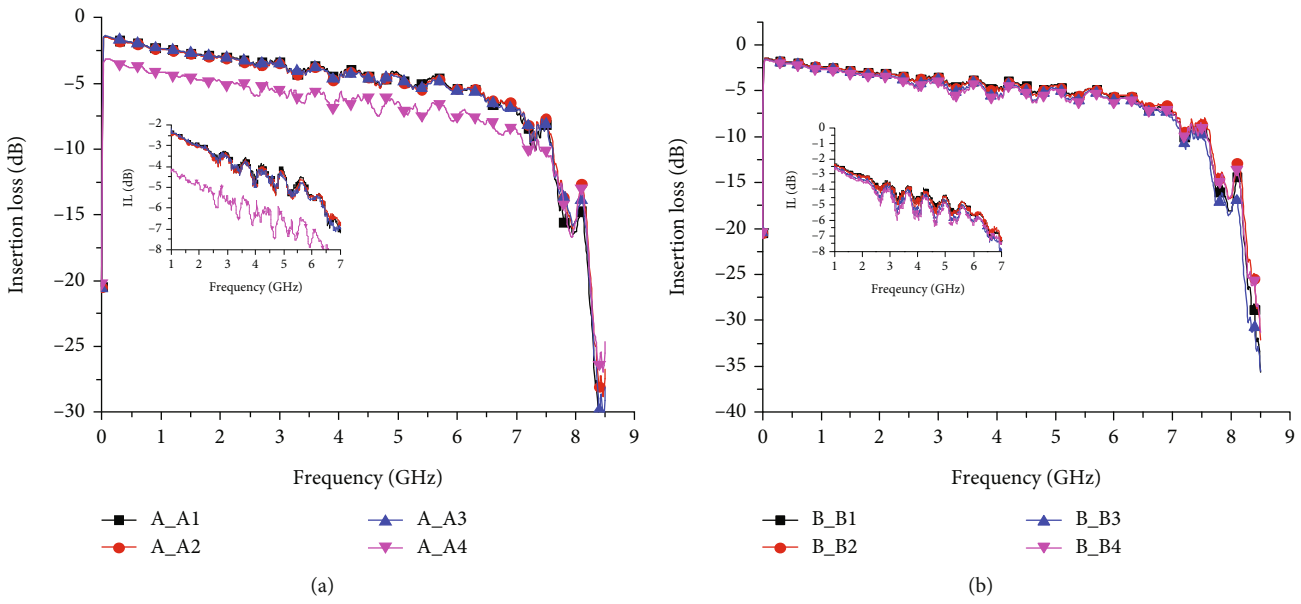

Figure 3: Measured insertion loss of the switch matrix: (a) Tx stage and (b) Rx stage.

6.0 GHz. This is caused by the SPDT switch not exhibiting sufficient performance due to the bandwidth of the operating frequency of 0.5–6 GHz [12].

2.2.2. Return Loss. The reflection loss is the lost value caused by reflected waves generated from the connector connection part of the cable.

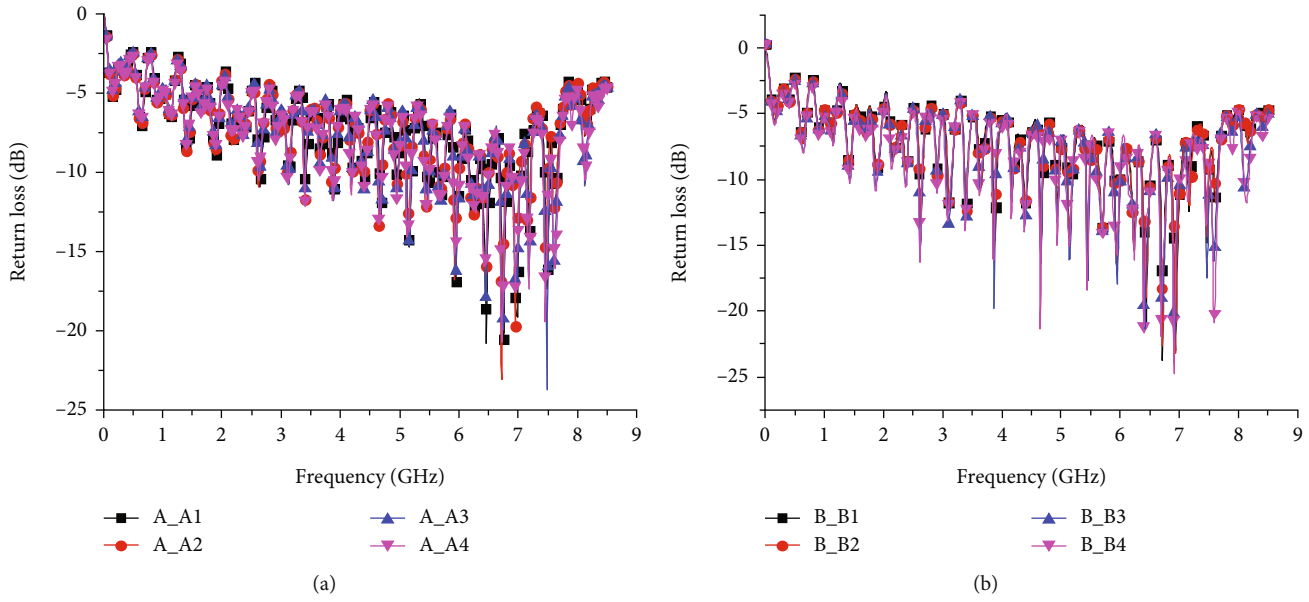

Figure 4: Measured return loss of the switch matrix: (a) Tx stage and (b) Rx stage.

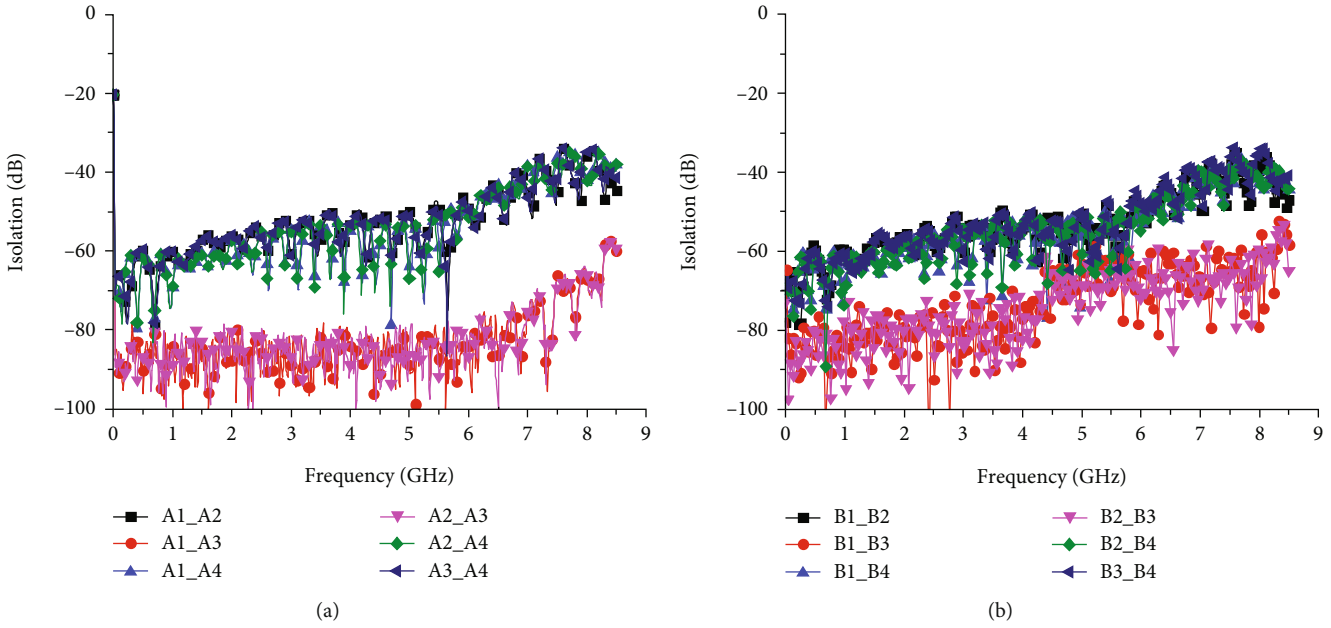

Figure 5: Measured isolation of the switch matrix: (a) Tx stage and (b) Rx stage.

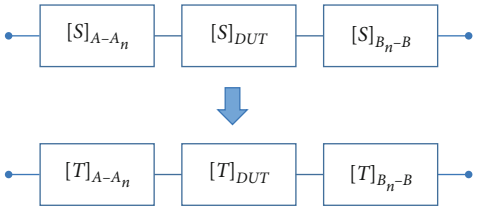

Figure 6: Transformation from S-parameter to T-matrix.

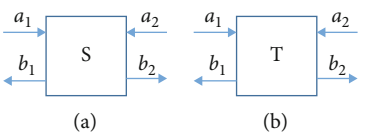

Figure 7: Diagram of (a) S-parameter matrix and (b) T-matrix.

Figure 4(a) shows the reflection loss of the Tx stage path composed of A-A_n, and Figure 4(b) shows the reflection loss of the Rx stage path composed of B-B_n. The four Tx and Rx

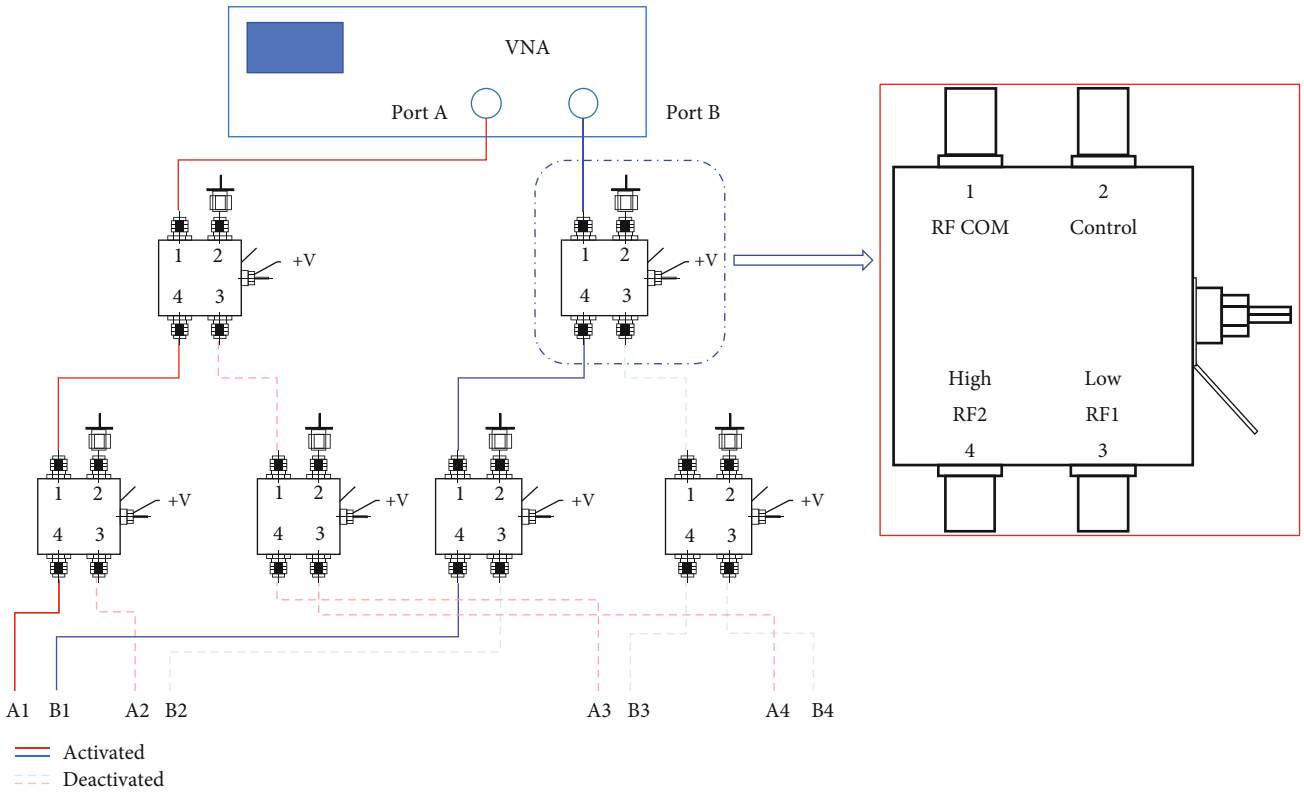

Figure 8: Schematic for the *S*-parameter measurement of channel 1.

terminal paths show different reflection loss tendencies up to 6 GHz, indicating a deterioration in reflection loss at a certain point when passing through several RF switches, RF cables, and RF connectors.

2.2.3. Isolation. Isolation represents the degree to which a signal affects a neighboring channel in a system with two or more channels. Figure 5(a) shows the isolation of the Tx stage path composed of A-A_n, and Figure 5(b) shows the isolation of the Rx stage path composed of B-B_n. The isolation results show that they are not identical due to RF cabling and connecting errors in manufacturing.

3. Calibration Method of Switch Matrix

The channel differences in insertion loss and reflection loss in an operating bandwidth are confirmed during the operation of the multiuser switch matrix, as shown in a previous section. This means that the de-embedding calibration method is required for each path when switching the multiuser switch matrix to another port. However, using manual calibration equipment is very slow, and it cannot be applied to high-speed switching. In addition, when calibration is performed using E-Cal equipment, calibration from one of the four channels causes the other three channels to be invalidated.

To solve this problem, calibration information for each channel is stored on the master PC to implement calibration in the program when the channel is changed. The performance of the implemented automatic calibration is checked through periodic tests.

The de-embedding calibration uses a method of obtaining data (S_{tot}) by connecting the DUTs to the Tx and Rx terminals of one channel of the switching matrix, obtaining the data (A-A_n, B_n-B, $n = 1, 2, 3, 4$) of the Tx and Rx stages, respectively, and correcting them. Here, since the *S*-parameter data measured by the VNA is in the form of a matrix in which the inversion cannot be directly calculated, a *T*-matrix is used (see Figure 6). Figure 7 shows the diagrams of the *S*-parameter and T-parameter for 2×2 input and output, respectively.

The matrices of the *S*-matrix and the *T*-matrix are expressed as follows.

$$\begin{bmatrix} b_1 \\ b_2 \end{bmatrix} = \begin{bmatrix} S_{11} & S_{12} \\ S_{21} & S_{22} \end{bmatrix} \begin{bmatrix} a_1 \\ a_2 \end{bmatrix}, \quad \begin{bmatrix} a_1 \\ b_1 \end{bmatrix} = \begin{bmatrix} T_{11} & T_{12} \\ T_{21} & T_{22} \end{bmatrix} \begin{bmatrix} b_2 \\ a_2 \end{bmatrix}. \tag{1}$$

Here, the coefficients of *T*-matrix can be obtained as follows [10].

$$[T] = \begin{bmatrix} \frac{1}{S_{21}} & -\frac{S_{22}}{S_{21}} \\ \frac{S_{11}}{S_{21}} & -\frac{S_{12}S_{21} - S_{11}S_{22}}{S_{21}} \end{bmatrix}. \tag{2}$$

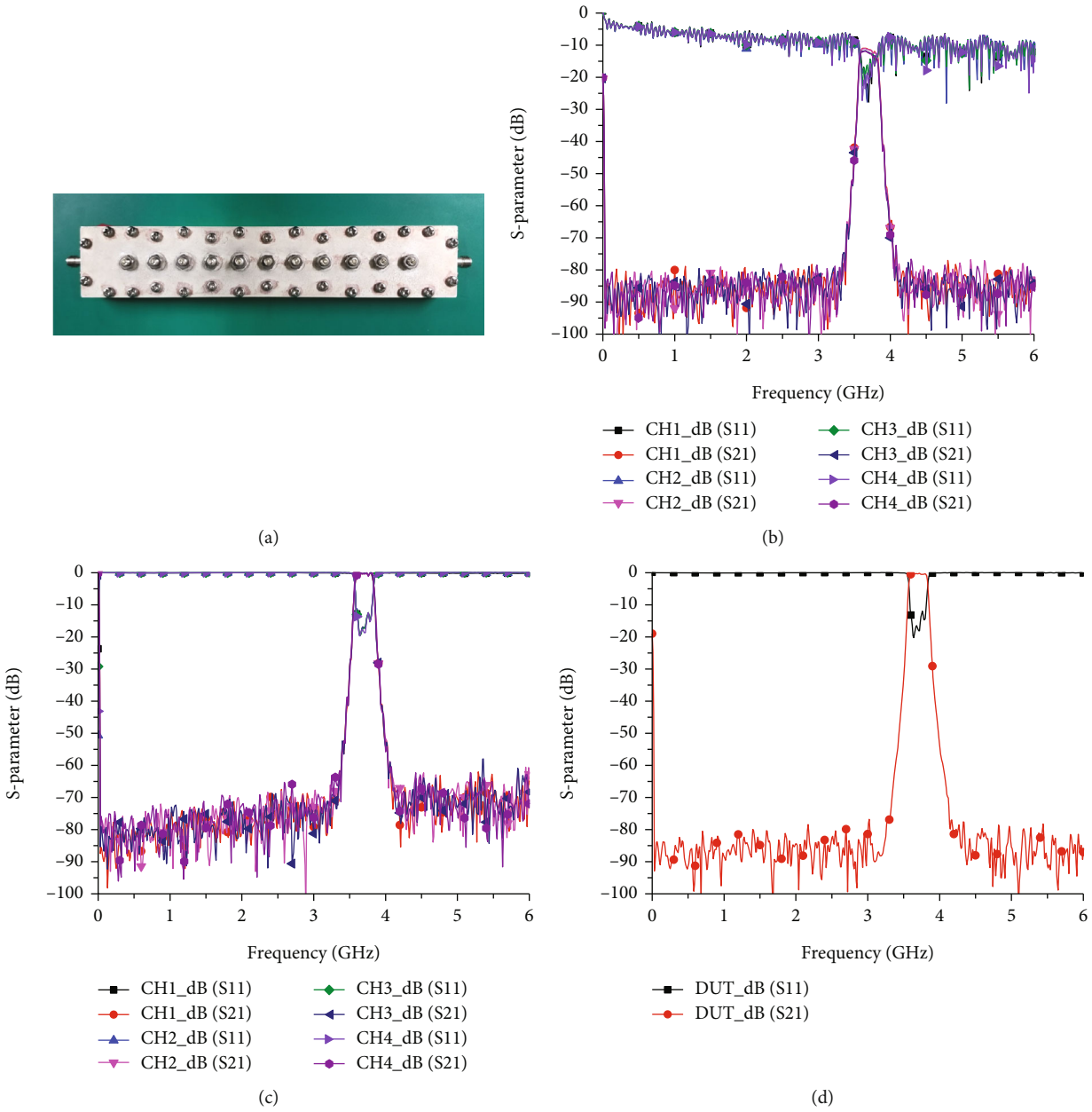

FIGURE 9: Performance test of the proposed de-embedding calibration: (a) 3.5 GHz RF cavity filter used as DUT, (b) measurement results before calibration, (c) measurement results applying the proposed de-embedding calibration, and (d) results measured by directly connecting the DUT to the calibrated VNA.

And then, T_{DUT} can be obtained by taking the T-matrix of the Tx and Rx stages converted in the inverse matrix on both sides of T_{tot} (see the following equations).

$$[T_{\mathrm{tot}}] = [T_{A\text{-}A_n}][T_{\mathrm{DUT}}][T_{B_n\text{-}B}], \tag{3}$$

$$[T_{\mathrm{DUT}}] = [T_{A\text{-}A_n}]^{-1}[T_{\mathrm{tot}}][T_{B_n\text{-}B}]^{-1}. \tag{4}$$

The formula in (5) is a relational expression with a T-matrix based on the S-parameter.

$$[S_{\mathrm{DUT}}] = \begin{bmatrix} \dfrac{T_{21}}{T_{11}} & \dfrac{T_{11}T_{22-}T_{21}T_{12}}{T_{11}} \\ \dfrac{1}{T_{11}} & -\dfrac{T_{12}}{T_{11}} \end{bmatrix}. \tag{5}$$

In this way, T_{DUT} is converted into S_{DUT}. Through this process, it is possible to calculate the S_{DUT} of all four channels. On the other hand, Figure 8 shows the example for the S-parameter measurement of specific channel.

4. Result of De-embedding Calibration

To implement de-embedding calibration for each channel, *S*-parameter data, including DUT, Tx stage, and Rx stage, are obtained for each channel before using the de-embedding algorithm. The *S*-parameter data of the channel1 is obtained using a schematic diagram, as shown in Figure 8. The *S*-parameter of the DUT is then calculated through each *S*-parameter measured using the de-embedding method.

The measurement process of the developed multiuser switching system is performed to confirm the validity of the de-embedded calibration. The de-embedded method is verified by comparing the *S*-parameter data of the DUT with the calculation values obtained from the de-embedding calibration and the Tx and Rx terminals of the VNA through the calibration kit.

To verify the calibration validity of the de-embedded calibration function, the *S*-parameter data of the DUT obtained by directly connecting the DUT to the calibrated VNA are compared with the *S*-parameter data of the DUT obtained by calculation using the de-embedding method.

Figure 9(a) shows the RF cavity filter passing at 3.5 GHz as a DUT. The measured results without the de-embedded calibration function are shown in Figure 9(b). Therefore, the unapplied de-embedding calibration results according to the four channels have distorted performances compared with the DUT results. Figure 9(c) shows the proposed de-embedding calibration method of Ch1 to Ch4. Figure 9(d) shows the measured results of de-embedded DUT using the conventional calibration method using VNA.

The graph of the de-embedding calibration method fits the DUT well below the 6 GHz frequency band. Therefore, the proposed development of a multiuser switching system is verified. When multiusers use the VNA, measurements can be performed without being affected by the signal path. Other DUTs within this frequency range can also be used, as we have shown good results with 6 GHz de-embedding.

5. Conclusion

In this paper, an RF switch matrix system for multiusers is developed to increase the number of VNA ports and accelerate the calibration speed to alleviate the equipment cost problem for multiusers. The developed switching matrix system is for a four-user switching system. An automatic de-embedding calibration algorithm is proposed to solve the nonidentity between each channel of the multiuser switch matrix. To verify the proposed RF switching system, the Tx and Rx channel performances are measured before and after using the de-embedding calibration method. When comparing the presence with the absence of de-embedding calibration method using DUT, the results of applying de-embedding are in good agreement with the DUT and effective in the switch operating range up to 6 GHz.

Data Availability

The data used to support the findings of this study are included within the article.

Conflicts of Interest

The authors declare that there are no conflicts of interest regarding the publication of this paper.

Acknowledgments

This research was supported by the MSIT (Ministry of Science and ICT), Korea, under the ICAN (ICT Challenge and Advanced Network of HRD) program (IITP-2024-2020-0-01832) supervised by the IITP (Institute of Information & Communications Technology Planning & Evaluation) and the Soonchunhyang University Research Fund.

References

[1] N. R. Franzen and R. A. Speciale, "A new procedure for system calibration and error removal in automated S-parameter measurements," in *1975 5th European Microwave Conference*, pp. 69–73, Hamburg, Germany, 1975.

[2] K. I. Silvonen, "A general approach to network analyzer calibration," *IEEE Transactions on Microwave Theory and Techniques*, vol. 40, no. 4, pp. 754–759, 1992.

[3] H. Heuermann, "Multiport S-parameter calculation from two-port network analyzer measurements with or without switch matrix," in *2006 67th ARFTG Conference*, pp. 219–222, San Francisco, CA, USA, 2006.

[4] J. C. Tippet and R. A. Speciale, "A rigorous technique for measuring the scattering matrix of a multiport device with a 2-port network analyzer," *IEEE Transactions on Microwave Theory and Techniques*, vol. 30, no. 5, pp. 661–666, 1982.

[5] I. Rolfes and B. Schiek, "Measurement of the scattering-parameters of planar multiport devices," in *2005 European Microwave Conference*, pp. 721–724, Paris, France, 2005.

[6] O. V. Drozd and D. V. Kapulin, "Metrological assistance of multiport vector network analyzers for microwave measurements," in *2018 XIV International Scientific-Technical Conference on Actual Problems of Electronics Instrument Engineering (APEIE)*, pp. 204–208, Novosibirsk, Russia, 2018.

[7] L. Zappelli, "Reconstruction of the S-matrix of N-port waveguide reciprocal devices from 2-port VNA measurements," *Progress in Electromagnetics Research B*, vol. 72, pp. 129–148, 2017.

[8] J. P. Dunsmore, *Handbook of Microwave Component Measurements, with Advanced VNA Techniques*, Wiley, 2nd edition, 2020.

[9] *Rohde & Schwarz ZNBT20 Manuals*, https://www.rohde-schwarz.com/us/manual/r-s-znb-znbt-user-manual-manuals_78701-29151.html and https://scdn.rohde-schwarz.com/ur/pws/dl_downloads/pdm/cl_manuals/user_manual/1173_9163_01/ZNB_ZNBT_UserManual_en_65.pdf.

[10] T. Holzmann, G. Batistell, H. Sterner, and J. Sturm, "Algorithms for de-embedding of RF measurement data for balanced and unbalanced setups," in *Proceedings of the 52nd Conference on Microelectronics, Devices and Materials (MIDEM)*, pp. 1–6, Slovenia, 2016.

[11] Mini-Circuits, *ZFSWA2R-63DR+ Data Sheet*, Data sheet, Brooklyn, NY, USA, 2016.

[12] W. Lee and S. Hong, "Frequency-reconfigurable SP4T switch with plaid metal transistors and forward body biasing for enhanced RON × COFF characteristics," *IEEE Transactions on Circuits and Systems II: Express Briefs*, vol. 69, no. 2, pp. 399–403, 2022.